Iosipescu Shear Deformation and Fracture in Model Thermoplastic Polyolefins

C. XIANG, H.-J. SUE

Polymer Technology Center, Department of Mechanical Engineering, Texas A&M University, College Station, Texas 77843-3123

Received 13 July 2000; accepted 6 October 2000

ABSTRACT: Shear deformation and fracture behaviors in polypropylene (PP)-based model thermoplastic polyolefins (TPOs) were investigated with the Iosipescu shear test. The shear deformation process was monitored *in situ* via video camera to obtain experimental shear stress–strain curves of model TPOs. Shear fracture mechanisms were studied with optical microscopy and scanning electron microscopy. Macroscopically, the cracks in neat PP propagated along the maximum shear plane, which indicated that mode-II shear failure existed in neat PP. Microscopically, it was shown that shear fracture initiated in the form of partial, discontinuous inclined microcracks that later coalesced and formed the final continuous crack. The incorporation of rubber in PP could transform the shear fracture process into a stretching process in the shear damage zone. © 2001 John Wiley & Sons, Inc. J Appl Polym Sci 82: 3201–3214, 2001

Key words: Iosipescu test; thermoplastic polyolefins; fracture mechanism; shear deformation; polypropylene

INTRODUCTION

Thermoplastic polyolefins (TPOs) show considerable promise for automotive applications because of their inherent performance advantages, particularly their weatherability, recyclability, and low cost. TPOs are currently utilized for interior instrument panels, bumper fasciae, and so on. The ability of these materials to resist scratching is of great interest.[1–3] Recent studies on the fundamental mechanics of the scratch/wear process[4–8] have clearly indicated that mode-II shear failure on the surface and subsurface is one of the main scratch-damage features. This damage process can lead to premature failure under some conditions and may limit the service life of the products. Therefore, the study of shear-induced fracture in TPOs is of considerable importance. Mode-I fracture behavior of high performance TPOs has been widely studied.[9–15] However, there has been little attention focused on shear deformation and fracture in TPOs. A fundamental investigation of the shear behavior in TPOs is needed. Such an investigation would be helpful for the development of shear-fracture-resistant and scratch-resistant TPOs.

Good experimental methods for studying shear deformation behavior are scarce. Commonly utilized tests include lap shear, napkin ring, end-notch flexure beam, puncture, Iosipescu, and torsion of a thin-walled tube.[16–23] Some of the above test methods are suitable for bulk materials, and others are for adhesives or composite laminates. Considering both the uniformity of stress distribution and the simplicity for specimen fabrication and experimental setup, the Iosipescu test was chosen here to study the shear deformation and fracture in model TPOs.

Correspondence to: H.-J. Sue (hjsu@acs.tamu.edu).

Contract grant sponsor: Defense Logistic Agency; contract grant number: SPO 103-96-D-0023.

Journal of Applied Polymer Science, Vol. 82, 3201–3214 (2001)

The Iosipescu shear test was originally developed for testing metals[16] and has become a generally accepted method for measuring the in-plane shear response of composites.[17–20] Recently, Liu and Piggott[22–24] carried out the Iosipescu test on a wide range of neat polymers. Shear fracture does not easily occur in many experimental setups and material combinations because cracks tend to propagate in the direction normal to the maximum principal stress (i.e., mode-I dominant fracture). Nevertheless, mode-II fracture has been shown to occur in some materials in a shear-loaded beam with a starter notch.[25]

The objective of this work was to study the shear fracture process in model TPOs under uniformly applied shear loading. Samples with and without sharp starter precracks were used to investigate shear deformation and shear crack growth with the Iosipescu shear test. Optical microscopy (OM) and scanning electron microscopy (SEM) were used to reveal the shear failure process in TPOs.

EXPERIMENTAL

Materials

A set of polypropylene (PP)-based model TPOs was received from ATC Corp. The neat PP (Aristech D-080-a2), with a melt flow rate index (MFR) of 8, was used as the matrix. The ethylene–propylene rubber (EPR) (Japan Synthetic Rubber EP02P), with a MFR of 3.2, was incorporated as the toughener phase. Fine talc particles (Luzenac Cimpact 710), with a median diameter of 1.5 μm, were used as rigid fillers in the TPOs. Specimens of neat PP, blends of PP and EPR, and PP, EPR, and talc, each with 10% by weight addition, were injection-molded into tensile and Iosipescu bars.

For comparison purposes, brittle polystyrene (PS) samples (Chevron EB3300) were also studied with the Iosipescu test.

Iosipescu Test

The geometry of the Iosipescu specimens employed in this investigation is given in Figure 1. To ensure proper alignment of the two notches, samples were notched carefully with a notch cutter to form a 90° angle notch with a depth of 2.54 mm on each side of the bar. To study the mode-II fracture behavior, samples with and without sharp cracks were prepared for comparison purposes. A pair of sharp precracks were made by a serrated razor blade, and then the sample was tapped with a liquid-nitrogen-chilled razor blade to open a sharp crack and to prevent significant yielding in front of the crack tip. The distance between the two notch tips was set to be 6 mm.

The Iosipescu test fixture was modified from the Wyoming fixture.[17–19] A schematic of the Iosipescu shear force diagram is shown in Figure 1(b). The instrumentation of the Iosipescu test used in this study is illustrated in Figure 2. The test was conducted at a constant crosshead speed of 2.54 mm/min with a computerized Sintech screw-driven mechanical testing machine.

To obtain the shear stress–strain curves during the shear test, the shear deformation behavior was monitored *in situ* with a stereo optical microscope with magnifications up to 50×; the microscope was attached to a video camera during the test. Image-capturing software (Optimas, version 6.2), which captures one image per second, was used for image processing and analysis. To facilitate the quantitative determination of the shear stress–strain curve, fine orthogonal grid lines were manually inscribed on the surface of the ligament region of the specimen [Fig. 1(b)]. The average length between these reference grids before loading was 1 mm. The shear strain γ was calculated according to the following equation:

$$\gamma = \tan \theta$$

where θ is the inclination angle against the horizontal grid lines. The average of the slopes of three horizontal lines on each image was used to calculate the shear strain. The shear stress, τ was defined as

$$\tau = \frac{P}{l \times t}$$

where P is the shear load, l is the ligament of the specimen, and t is the thickness of the specimen. With this instrumentation setup, an accurate experimental shear stress–strain curve was generated.

Microscopy

To characterize the shear fracture features in TPOs, both the fracture surface features of the failed samples and the subsurface damage of the partially failed samples were probed.

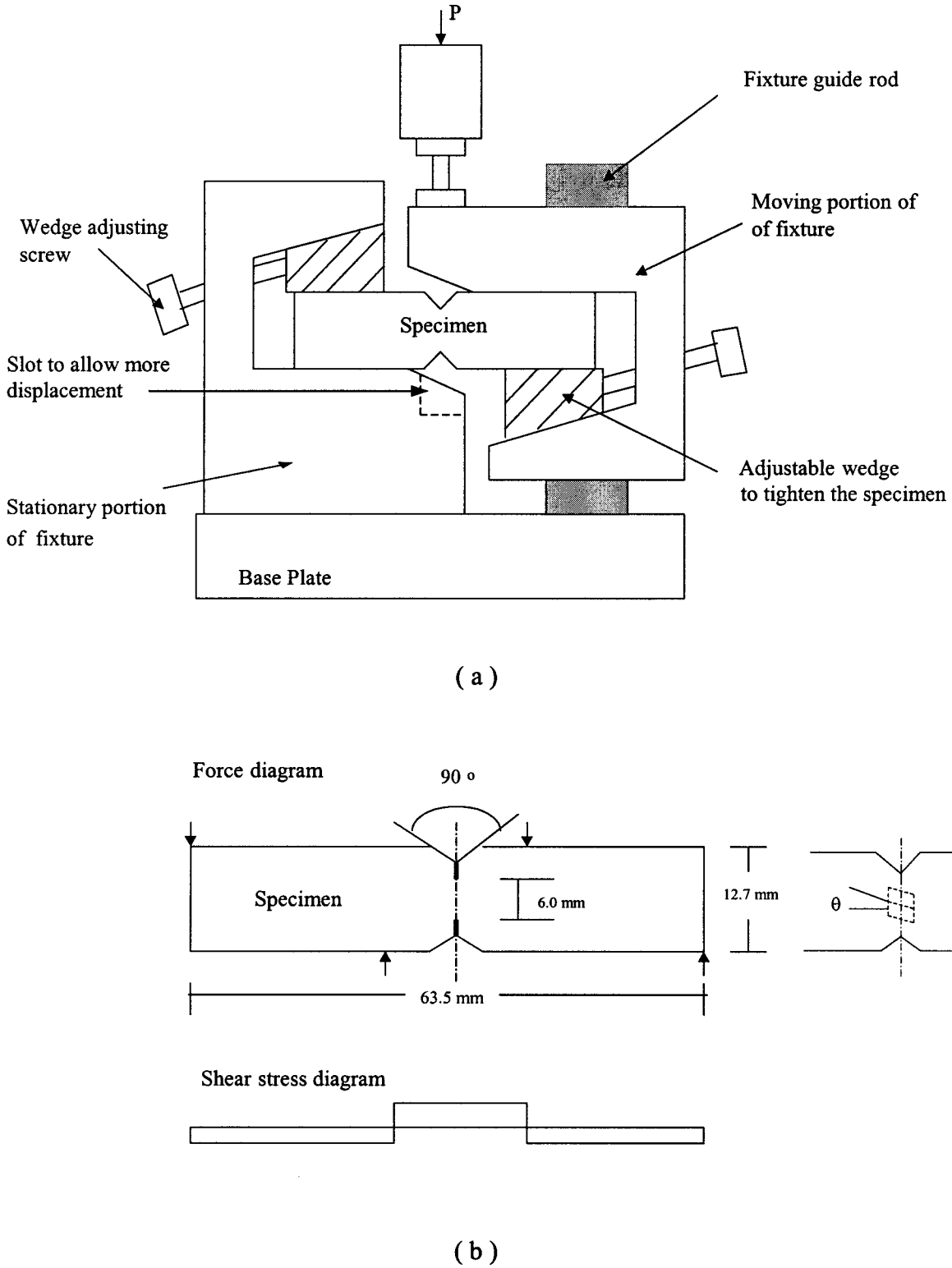

Figure 1 (a) Schematic of the Iosipescu shear test fixture (ASTM D5379M) and (b) idealized force and shear stress diagram and geometry of the specimen.

This was done with techniques similar to those used to characterize mode-I damage mechanisms.[26]

The shear fracture surfaces of the failed specimens were coated with Au–Pd and studied with a JSM-6400 scanning electron microscope,

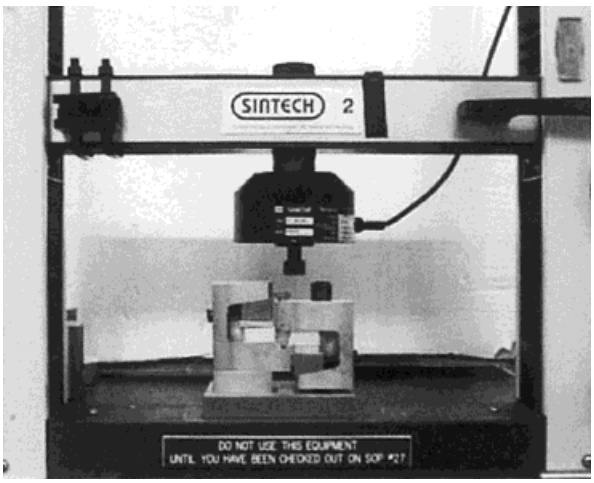

Figure 2 Photograph of the Iosipescu shear test setup.

which was operated at an accelerating voltage of 15 kV.

The samples containing shear damage that did not fail completely were cut in half along the shear crack propagation direction (Fig. 3). The first half of the damaged sample was finely polished and was then adhered to a glass slide with an epoxy adhesive. After the adhesive had cured, the remaining sample was cut off and polished to a thickness of about 20 μm. The sample was then polished with a 0.3 μm Al_2O_3 size aqueous emulsion to obtain a good quality thin section for transmitted optical microscopy (TOM) observation. TOM thin sections were then examined with an Olympus BX60 optical microscope under both bright field and crossed polars.

The other half of the damaged sample was polished to a 0.5 μm Al_2O_3 size aqueous emulsion surface finish on the midplane to obtain a flat, smooth surface. Then, the polished samples were immersed overnight in an etching solution that contained 1.3 wt % potassium permanganate, 32.9 wt % H_3PO_4, and 65.8 wt % concentrated H_2SO_4.[27,28] The amorphous phase and the rubber particles were etched preferentially and could be easily revealed with SEM. SEM was performed to study the detailed shear damage mechanisms after etching.

For reference, some unetched samples were also polished and studied with electroscan environmental scanning electron microscopy (ESEM; model E-3 from FEI Co.) to identify the damage mechanisms.

RESULTS

Typical shear load-displacement curves of model TPOs without sharp precracks are shown in Figure 4. All specimens showed plateaus after the apparent yielding point (peak load). The neat PP specimen exhibited a small amount of load drop. The load drop was not observed in other specimens. All specimens showed slight strain hardening characteristics.

Typical shear load-displacement curves of model TPO systems with sharp precracks are shown in Figure 5. It is obvious that the maximum shear failure strains achievable by different materials under the same test conditions were different. Neat PP failed at a lower strain, whereas the EPR toughened samples, with and without talc filler, exhibited a much larger strain to failure. These results indicate that the unmodified PP system was more flaw (notch) sensitive under shear test. In addition, the neat PP specimen exhibited quite a sudden load drop after the peak load was reached, whereas PP/EPR stayed flat after the apparent load peak. PP/EPR/talc showed a gradual decrease in load until the end of the test.

Obtained with the aid of *in situ* video camera observation and image analysis, typical experimental shear stress–strain curves of model TPOs are given in Figure 6. Typical images, captured by the camera through OM, of the shear deformation of neat PP at different time during the test are shown in Figure 7. To evaluate the shear property of the model TPOs, samples with two different thickness values [i.e., 3.175 mm (0.125 in.) and 2.032 mm (0.08 in.)] were also conducted. Table I compares the yield stresses obtained from the Iosipescu shear test and the tensile test. The yield stress in the Iosipescu shear test was defined as the onset load of the plateau in the load-displacement curve (see arrows in Fig. 4) divided by the corresponding area (thickness $\times$ ligament length). The equivalent shear yield stress based on the tensile test was converted with the von

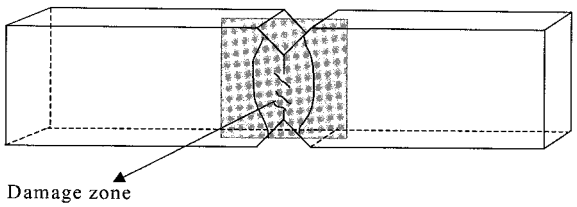

Figure 3 Sections cut from damaged samples for TOM and SEM investigations.

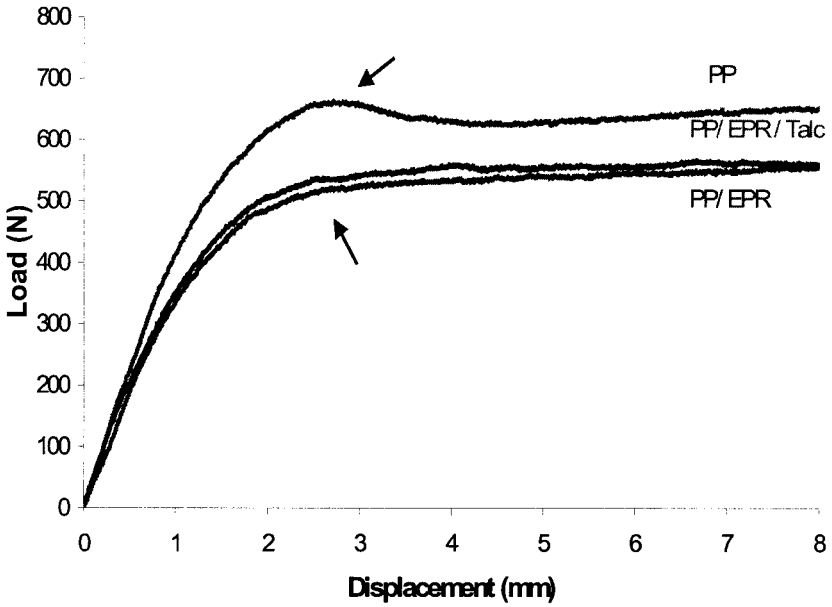

Figure 4 Typical load-displacement curves of model TPOs without sharp precracks. The arrows indicate the onset of the plateau portion of the curve.

Mises yield criterion ($\tau_s = Y/\sqrt{3}$, where τ_s and Y are the yield stresses in pure shear and in tension, respectively). As seen from Table I, when the thickness was small, the yield stress values obtained from the Iosipescu shear test and the tension test were close to each other. This indicates that the model TPO systems basically obeyed the von Moses yield criterion. A detailed discussion concerning the effect of thickness on the Iosipescu shear test will be reported in a subsequent publication.

Because the testing results in Figures 4 and 5 show different shear fracture behaviors among the model TPO systems, the shear fracture mechanisms among them were expected to be different. Figure 8 shows the overall shear fracture patterns of the TPOs tested. For comparison, PS samples were also tested after the same testing procedures. Three types of shear fracture patterns were observed on the tested specimens. For PS, two approximately parallel macroscopic cracks, starting at the precrack tip and orientating at approximately 48°

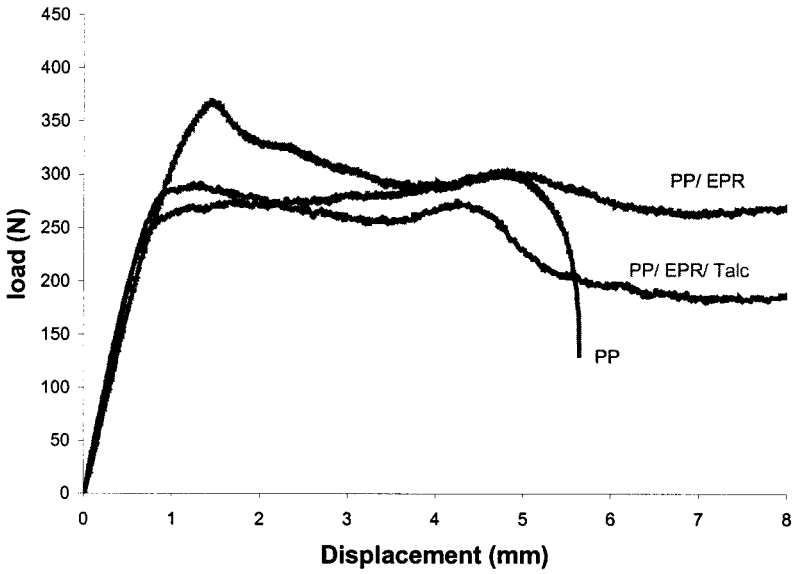

Figure 5 Typical load-displacement curves of model TPOs with sharp precracks.

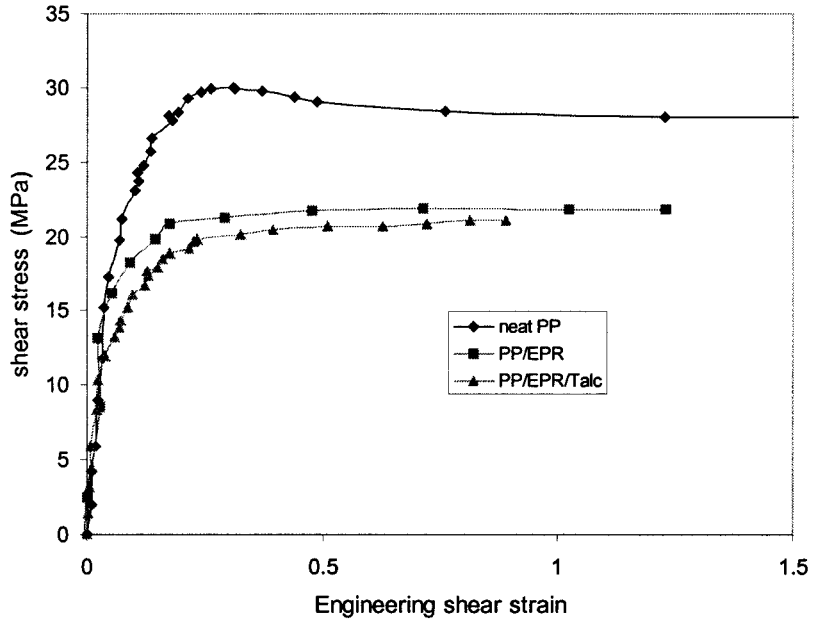

Figure 6 Experimental shear stress–strain curves of model TPOs.

from the edge of the sample, ran across the entire sample. The angle coincided with the direction of the maximum principal tensile stress under shear loading. In addition, the crack propagated unstably once it started. No sign of plasticity was seen in the sample.

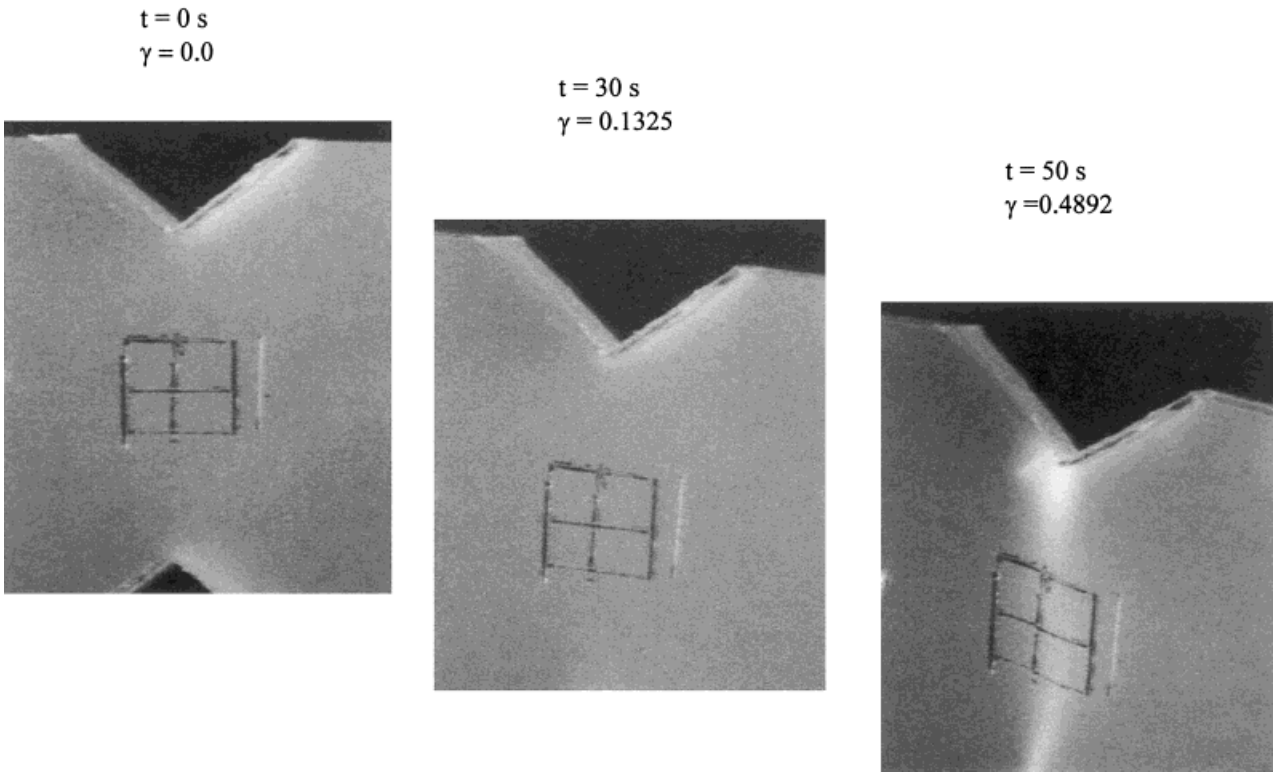

Figure 7 Typical images captured from OM showing shear deformation during the Iosipescu shear test for neat PP.

Table I Comparison of the Yield Stresses Obtained with the Iosipescu Shear Test and the Tensile Test

	Yield Stress Under Tension (MPa)	Yield Stress in Pure Shear for Samples with Different Thicknesses (MPa)		Estimation of Yield Stress Based on von Mises Yield Criterion (MPa)
		3.175 mm	2.032 mm	
PP	38.72	30.03	24.91	22.35
PP/10% EPR	33.41	21.08	19.51	19.28
PP/10% EPR/10% Talc	35.23	21.55	20.45	20.33

However, the model TPOs showed different shear fracture patterns. A macroscopic crack was seen in neat PP. The crack propagated directly along the neck section of the sample, which followed the maximum shear stress direction, until final failure. A damage zone in the shear stress dominant region formed. The shear-induced crack experienced stable crack growth during loading until it failed. For rubber-toughened TPOs, with or without talc, there was no observable crack growth. Only the stretching of the neck section of the sample was found. A pronounced whitening in the damage zone was observed on the samples, which indicated cavitation was involved during the Iosipescu shear test.

Based on the previous findings, a schematic showing three types of failure modes in the Iosipescu shear test is summarized in Figure 9. They are mode-I failure (PS), mode-II failure (neat PP), and stretching failure in the notched region (rubber-toughened PP). Clearly, PP could fail in mode II during the applied shear stress state. Therefore, there was a need to study the fundamental mode-II fracture behavior in PP. To understand unambiguously the shear fracture mechanism in TPOs and determine the roles that the rubber particles and the rigid filler play in the shear fracture process, TOM and SEM techniques were employed.

An overview of the shear damage pattern via TOM thin sections under cross-polarized light and bright field is shown in Figures 10 and 11. Here, PP and PP/EPR/talc were chosen to demonstrate the shear damage mechanisms in detail. Figures 10 and 11 both exhibit a birefringent zone, indicating that there existed shear plastic deformation in the notched region during the Iosipescu shear test. For neat PP, some inclined microcracks were observed near the sharp precrack tip within the damage zone. For PP/EPR/talc, instead of the inclined microcracks, fibril formation could be seen (Fig. 11). Under cross-polarized light, PP/EPR/talc showed a much more extensive birefringence in the damage zone around the crack tips, which suggests that more extensive shear plastic deformation was present.

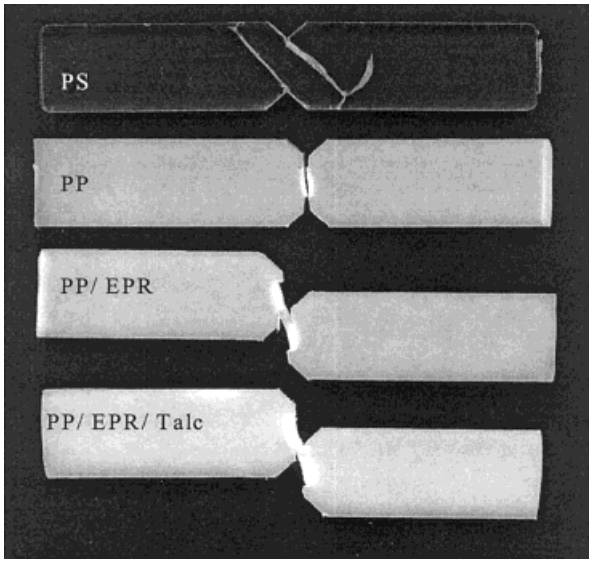

Figure 8 Overview of model TPOs and PS showing shear fracture patterns.

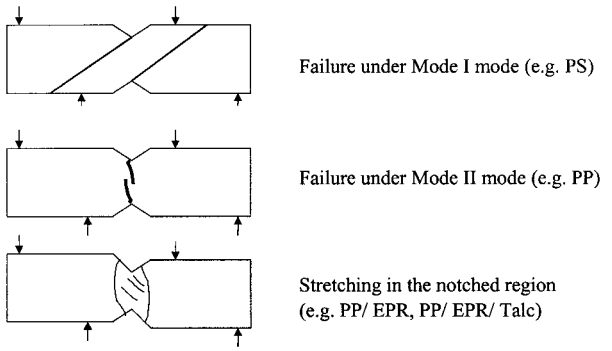

Figure 9 Schematic of typical shear fracture patterns observed in model TPOs and PS.

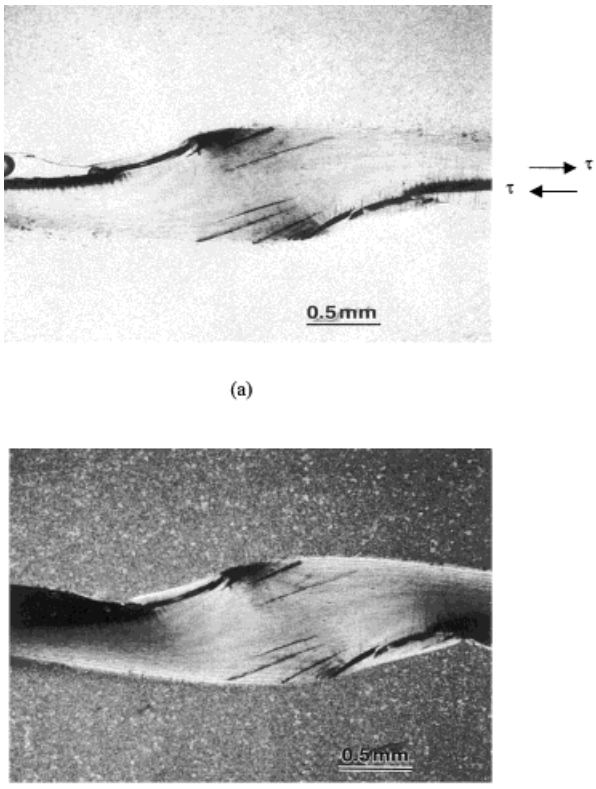

Figure 10 TOM thin section of a neat PP specimen taken under (a) a bright field and (b) cross-polarized light after an Iosipescu shear test.

Because of the low resolution of TOM, details of the damage mechanisms could not be observed unambiguously. SEM was conducted on the PP and PP/EPR/talc etched samples (Figs. 12 and 13). Under low magnification [Figs. 12(a) and 13(a)], the shear damage pattern was similar to that observed with TOM. Because features such as crazes, cracks, and the amorphous phase were preferentially etched away, cracklike features were more readily seen in neat PP. However, no crazes or microcracks were found in etched PP/EPR/talc. When the SEM micrograph of the shear damage zone was viewed under high magnification [Figs. 12(b) and 13(b)], both samples showed highly orientated fibril-like structures. Many apparent microcracks perpendicular to the orientated fibrils could be seen. For talc-filled TPOs, some debondings between the talc and the matrix were observed. Spherulites could not be easily observed in the damage zone. Under the same magnification, spherulites could be clearly seen in the damage-free zone of neat PP [Fig. 12(c)]. For comparison, an SEM micrograph of the damage-free zone of PP/EPR/talc is also shown in Figure 13(c).

The superstructure of isotactic PP was comprehensively reviewed by Varga.[29] The *in situ* observations of the deformation of PP spherulites and crystalline lamellae under simple shear with SEM and scanning force microscopy were intensively examined by Aboulfaraj, G'Sell, and others.[27,28] The deformation mechanisms of semicrystalline polymers were well-reviewed by Peterlin[30] and Lin and Argon.[31] Studies have shown that spherulites in PP can bear large shear deformation and conform to a highly elongated shape along the maximum principal strain axis until they form fibrils. These studies have also shown that the crystalline lamellae orientation is perpendicular to the stretching direction after severe drawing. As seen in Figures 12(b) and 13(b) from this study, it is suggested that the orientated fibril-like structures were formed under large shear strain. At this stage, it is still unclear what caused the formation of the observed fibril structure. It will be the subject of future investigation. However, the observed highly orientated structures do indicate that a high stretching process occurs during the shear test.

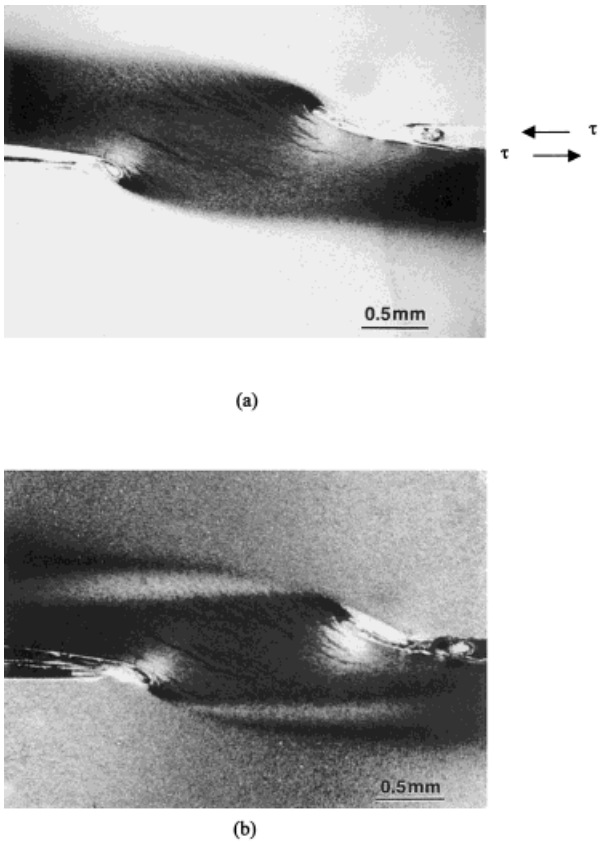

Figure 11 TOM thin section of a PP/EPR/talc specimen taken under (a) a bright field and (b) cross-polarized light after an Iosipescu shear test.

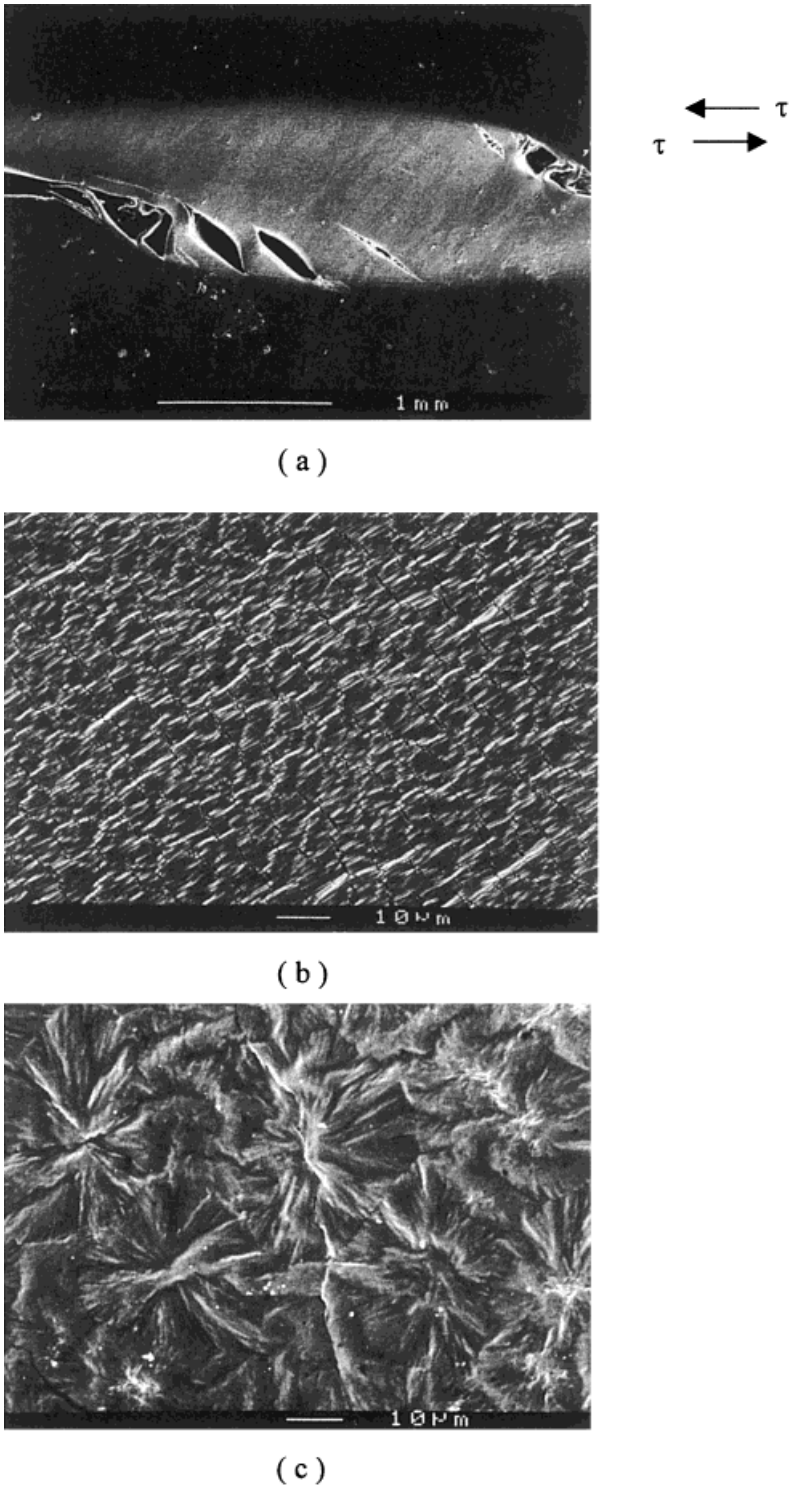

Figure 12 SEM micrographs of a neat PP specimen after an Iosipescu test: (a) an overview of the shear damage zone, (b) the damage zone, and (c) the undamaged zone.

To determine the effect of chemical etching and Au–Pd coating on the observed damage features, the unetched, polished PP sample with Au–Pd coating and the unetched PP/EPR/talc sample without Au–Pd coating were examined with SEM and ESEM, respectively, (Fig. 14). It is apparent that the main features observed in Figures 12 and 13 are shown again in Figure 14(a), suggesting

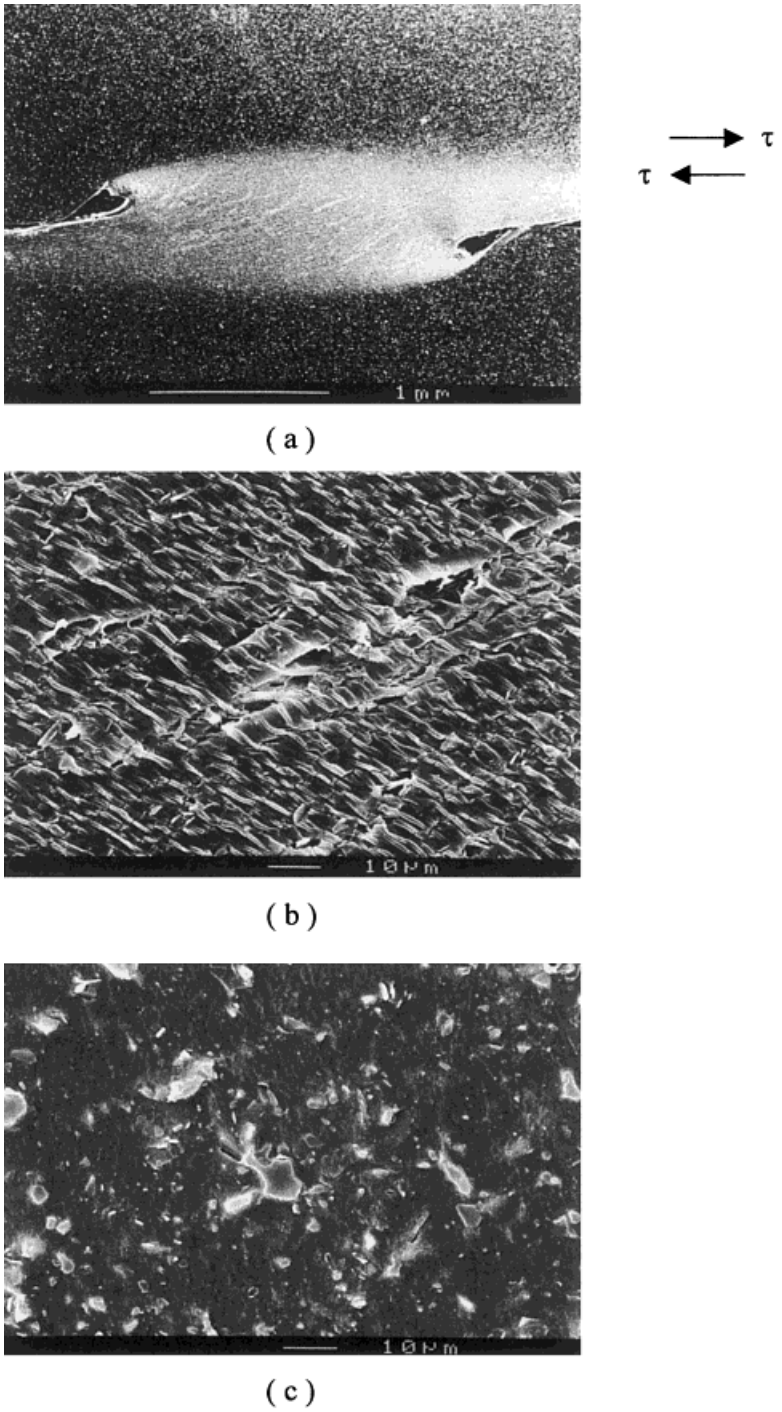

Figure 13 SEM micrographs of a PP/EPR/talc specimen after an Iosipescu test: (a) an overview of the shear damage zone, (b) the damage zone, and (c) the undamaged zone.

that stretching, in the form of highly orientated fibril-like structures, is the main damage feature in the Iosipescu shear damage test for TPOs. However, the multiple cracks perpendicular to the orientated fibrils observed in samples with Au–Pd coating were not found in the samples without Au–Pd coating [Fig. 14(b, c)]. This implies that the PP matrix can endure high shear deformation without inducing crack during the shear process. The multiple cracks found in the Au–Pd coated samples were, in fact, artifacts.

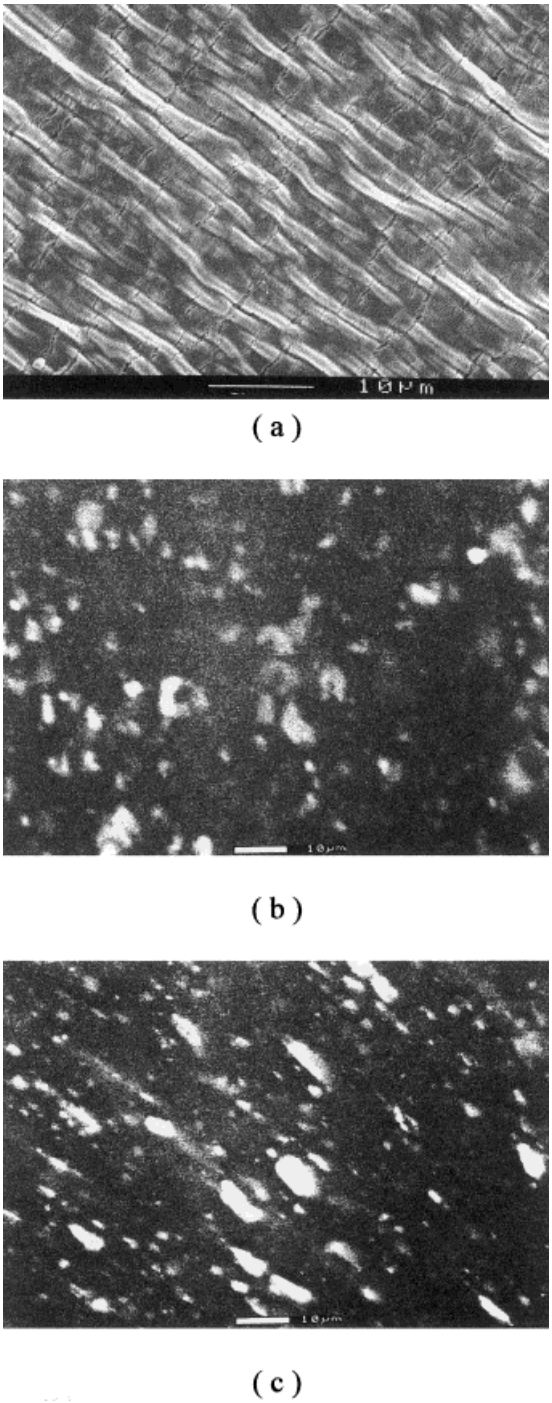

Figure 14 (a) SEM micrograph of PP without etching and ESEM micrographs of a PP/EPR/talc specimen without Au–Pd coating (b) in the damage-free zone and (c) in the damaged zone.

Shear fracture surfaces on all samples were studied by SEM (Figs. 15–17). In neat PP (Fig. 15), the fracture surface showed a smooth region, followed by a striated region, which was similar to the puncture fracture surface features reported by Liu and Piggot.[22] The smooth region indicated stable crack growth in the shear test. A high-magnification SEM micrograph taken in the smooth region about 450 μm away from the crack tip showed signs of widespread fibrils drawing on the fracture surface. PP/EPR showed a much more ductile failure mode (Fig. 16). The plastic flow and fibril formation were present during the beginning of the shear fracture, followed by macroscopic ductile stretching. A high-magnification SEM micrograph [Fig. 16(b)] taken in the fibril formation region further showed the plastic flow involved in the shear test. In the case of PP/EPR/talc, the fibril region ahead of the crack tip was not as large as that in PP/EPR sample, but it did show a stable ductile drawing (Fig. 17). High-magnification SEM micrographs for PP/EPR/talc

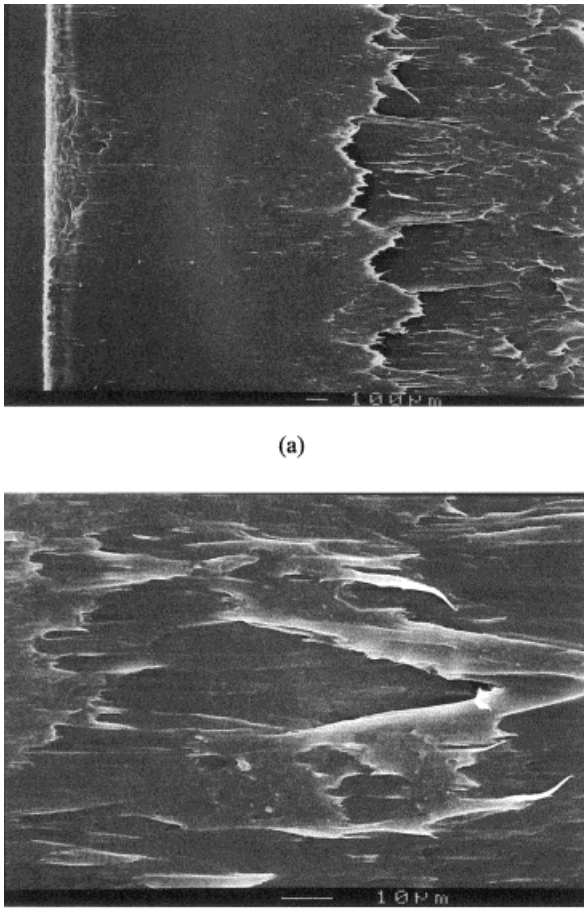

Figure 15 SEM micrographs of a neat PP specimen taken on the fracture surface after an Iosipescu test: (a) an overview of the fracture surface and (b) the stable crack-growth zone. The crack propagates from left to right.

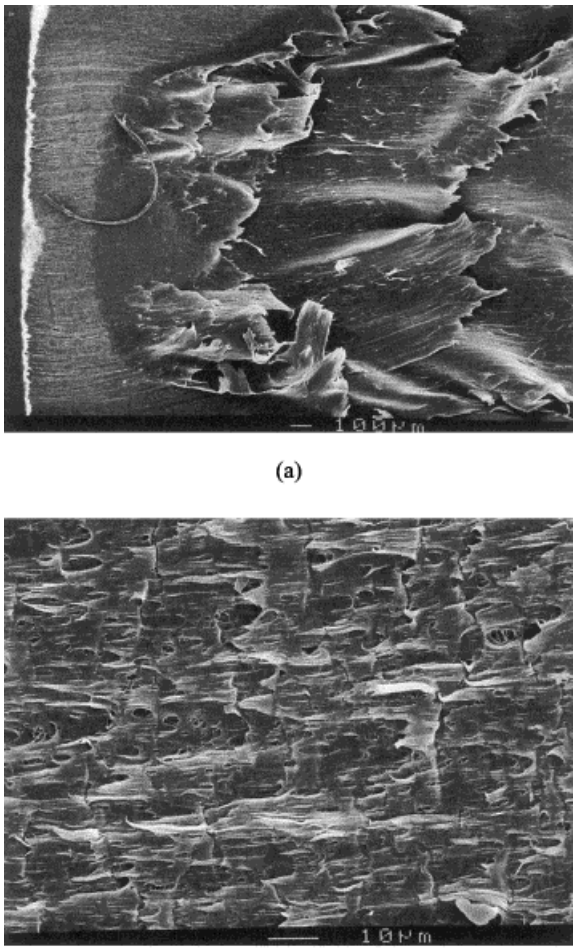

Figure 16 SEM micrographs of a PP/EPR specimen taken on the fracture surface after an Iosipescu test: (a) an overview of the fracture surface and (b) the stable crack-growth zone. The crack propagates from left to right.

showed highly ductile drawing during the shear test. Clearly, the debonding between the talc and the matrix suggests poor adhesion between them.

DISCUSSION

The study of mode-II crack propagation is difficult because mode-I crack growth can easily take over. It is known that mode-II growth, if it occurs, proceeds in the maximum shear stress direction. It has been reported by Bazant and Pfeiffer[25,32] that shear fracture occurs in concrete under the asymmetrical four-point bending (AFPB) shear test with two collinear edge precracks subjected to shear loading. In fact, the Iosipescu shear test is similar to the AFPB shear test [Fig. 1(b)]. Nonetheless, the concentrated stresses caused by the cylindrical loading points can be avoided[17] during the Iosipescu test. The nature of shear fracture was investigated by Bazant and Pfeiffer with finite element analysis based on the crack band model[25] and shear testing on various sample sizes. It has been shown that a pure mode-II situation exists at the crack tips during the shear test, at least in the beginning of the shear process. During shear loading, cracks are partially formed that consist of a band of distinct, discontinuous microcracks within a relatively large fracture process zone at the crack front.

For neat PP, macroscopically, the crack follows the maximum shear stress direction, which is straight along the neck section, indicating the dominance of mode-II shear fracture in PP. Mi-

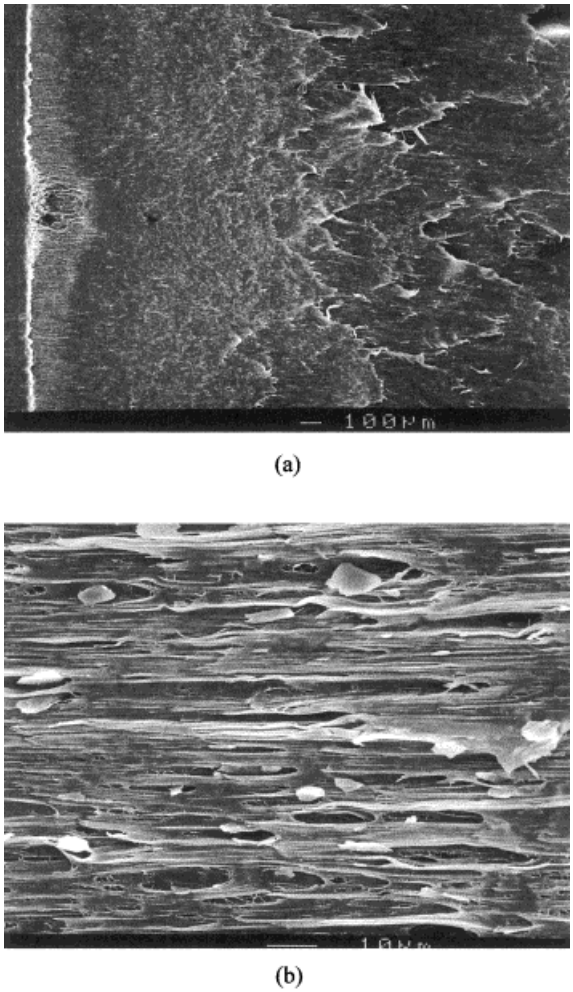

Figure 17 SEM micrographs of a PP/EPR/talc specimen taken on the fracture surface after an Iosipescu test: (a) an overview of the fracture surface and (b) the stable crack-growth zone. The crack propagates from left to right.

croscopically, it is evident that inclined bands of microcracks emanate from the sharp precrack tips and propagate continuously toward the center of the neck section. As seen from Figure 8, the angle of microcrack inclination from the notch becomes smaller when the crack forms toward the center of neck section. The presence of the inclined microcracks suggests that the shear fracture process is attributed to the maximum tensile stress in the beginning of the shear process. From the standpoint of fracture energy, the formation of inclined microcracks in the beginning of the shear process causes the release of some strain energy. This is consistent with the observation of load drop after the peak load is reached (Fig. 5). A highly stretched shear zone is formed between the notched regions, as indicated by the highly orientated fibril-like structure. When the running crack grows in the highly stretched zone, it can cause a significant release of strain energy. As the shear process continues, the final failure, which results from the connection of the microcracks, causes a sudden load drop in the load-displacement curve. The overall failure is dominated by shear.

For the PP/EPR and PP/EPR/talc systems, no inclined microcracks were observed. Therefore, there was no significant load drop observed in the load-displacement curve (Fig. 5), which means that no energy release occurred in the beginning of the shear process. This finding suggests that the high ductility of the matrix caused by rubber toughening dramatically reduced the chance of forming microcracks. A highly stretched zone was observed in the shear damage region of both PP/EPR and PP/EPR/talc, which was similar to those found in PP. No crack growth was observed in the highly stretched zone. A high distortional strain energy resulted from stretching the material during the shear process. By adding EPR to PP, the strain energy was dissipated by the stretching of material rather than through microcracking in the shear deformation zone.

With the addition of talc, debondings between matrix and talc particles occurred in the shear deformation zone, which further released strain energy during the shear process. SEM micrographs of the shear fracture surface indicated that widespread debonding took place. Clearly, a gradual decrease of load in the load-displacement curve can be partially attributed to the release of strain energy caused by debonding between the talc particles and the matrix. There was no macrocrack growth observed in PP/EPR/talc during the shear test.

CONCLUSIONS

Mode-II shear deformation and fracture behaviors of model TPOs were investigated with the Iosipescu shear test. Shear stress–strain curves of model TPOs were generated experimentally with the Iosipescu shear test. Macroscopically, shear fracture existed in PP. That is, the crack could propagate in the neck section, which was the maximum shear stress direction. TOM and SEM investigations of model TPOs gave a clear description of the shear fracture process, which was consistent with the work of Bazat and Pfeiffer with the crack band model. Microscopically, the shear fracture zone was composed of a collection of inclined microcracks, which were later connected by further shearing. In addition, a highly stretched zone, in the form of a highly orientated fibril-like structure, in the damage zone between the notches indicated that high distortional strain energy was involved during the shear process. The observed shear fracture energy was caused by the formation of inclined microcracks in the process zone and by stretching the material in the deformation zone. Neat PP was prone to shear fracture. The incorporation of rubber could suppress shear fracture mechanisms and promote a stretching mechanism because of the high ductility of rubber-toughened PP.

The authors thank Brian Coleman of ATC Co. for providing the model TPOs for this work.

REFERENCES

1. Chu, J.; Rumao, L.; Coleman, B. Polym Eng Sci 1998, 38, 1906.
2. Chu, J.; Xiang, C.; Sue, H.-J.; Hollis, R. D. Polym Eng Sci 2000, 40, 944.
3. Pickles, M. J.; Hutchings, I. M. Automot Automat Limited 1997, 391.
4. Komvopoulos, K.; Cho, S.-S. Wear 1997, 209, 57.
5. Xiang, C.; Sue, H.-J.; Chu, J. J Polym Sci Part B: Polym Physics 2001, 39, 47.
6. Komvopoulos, K. Wear 1997, 199, 9.
7. Klapperich, C.; Komvopoulos, K.; Pruitt, L. J Tribol 1999, 121, 394.
8. Sin, H.-C.; Suh, N. P. J Appl Mech 1984, 51, 317.
9. Chou, C. J.; Vijayan, D.; Kirby, D.; Hiltner, A.; Baer, E. J Mater Sci 1988, 23, 2521.
10. Chou, C. J.; Vijayan, D.; Kirby, D.; Hiltner, A.; Baer, E. J Mater Sci 1988, 23, 2533.
11. Jang, B. Z.; Uhlmann, D. R.; Vander Sande, J. B. Polym Eng Sci 1985, 25, 643.

12. Mouzakis, D. E.; Stricker, F.; Mulhaupt, R.; Karger-Kocsis, J. J Mater Sci 1998, 33 2551.
13. Masaru, I.; Masataka, S.; Toshio, I. J Appl Polym Sci 1996, 62, 1495.
14. Wei, G.-X.; Sue, H.-J.; Chu, J.; Huang, C.; Gong, K. Polymer 2000, 41, 2947.
15. Wei, G.-X.; Sue, H.-J.; Chu, J.; Huang, C.; Gong, K. J Mater Sci 2000, 35, 555.
16. Iosipescu, N. J Mater 1967, 2, 537.
17. Walrath, D. E.; Adams, D. F. Exp Mech 1983, 23, 105.
18. Adams, D. F.; Walrath, D. E. Exp Mech 1987, 27, 113.
19. Adams, D. F.; Lewis, E. Q. SAMPE J 1994, 31, 32.
20. Pindera, M.-J.; Ifju, P.; Post, D. Exp Mech 1990, 30, 101.
21. Chai, H. J Mater Sci 1993, 28, 4944.
22. Liu, K.; Piggott, M. R. Polym Eng Sci 1998, 38, 60.
23. Liu, K.; Piggott, M. R. Polym Eng Sci 1998, 38, 68.
24. Liu, K.; Piggott, M. R. Composites 1995, 26, 829.
25. Bazant, Z. P; Pfeiffer, P. A. Mater Struct 1989, 19, 111.
26. Sue, H.-J.; Yee, A. F. J Mater Sci 1993, 28, 2975.
27. Aboulfaraj, M.; G'Sell. C.; Ulrich, B.; Dahoum, A. Polymer 1995, 36, 731.
28. Coulon, G.; Castelein, G.; G'Sell, C. Polymer 1998, 40, 95.
29. Varga, J. J Mater Sci 1992, 27, 2557.
30. Peterlin, A. Colloid Polym Sci 1987, 265, 357.
31. Lin, L.; Argon, S. J Mater Sci 1994, 29, 294.
32. Bazant, Z. P.; Gambarova, P. G. J Struct Eng ASCE 1884, 110, 2015.